IEEE Access
Multidisciplinary | Rapid Review | Open Access Journal

Date of publication xxxx 00, 0000, date of current version xxxx 00, 0000.

Digital Object Identifier 10.1109/ACCESS.2017.DOI

An Electronically-Tunable, Flexible and Transparent Antenna with Unidirectional Radiation Pattern

ABU SADAT MD. SAYEM[1, 2], ROY B. V. B. SIMORANGKIR[3], (Member, IEEE), KARU P. ESSELLE[1], (Fellow, IEEE), DUSHMANTHA THALAKOTUNA[1], (Senior Member, IEEE), and ALI LALBAKHSH[2], (Member, IEEE)

[1]School of Electrical & Data Engineering, University of Technology Sydney, Australia.
[2]School of Engineering, Macquarie University, Sydney, Australia.
[3]Tyndall National Institute, University College Cork, Dyke Parade, T12R5CP Cork, Ireland.

Corresponding author: Abu Sadat Md. Sayem (e-mail: abusadatmd.sayem@uts.edu.au).

This work was supported in part by the Australian Research Council Discovery Grants Scheme and University of Technology Sydney Faculty of Engineering and IT Seed Grant.

ABSTRACT

In this paper, a frequency reconfigurable, conformal, durable, optically transparent, and unidirectional antenna design is demonstrated for the first time. In the demonstrated design, continuous frequency tuning is achieved by integrating a varactor diode in a folded dipole radiator, which is backed by a water-filled reflector to produce unidirectional radiation pattern mimicking the radiation characteristics of microstrip patch antennas. The radiating component of the explored antenna is manufactured from transparent conductive fabric, which has about 72% optical transparency and occupies a small fraction of the entire antenna. The water-filled reflector is located underneath the dipole radiator. Water is contained inside a rectangular box made from flexible-transparent-hydrophobic polymer, polydimethylsiloxane (PDMS). Both water and PDMS are highly transparent, moreover, PDMS has excellent flexibility and water is a liquid, thus, the demonstrated antenna exhibits excellent transparency and durability against physical deformation. The tiny varactor diode integrated in the folded dipole radiator has insignificant effect on the overall transparency and flexibility of the antenna. The explored design has been numerically investigated and experimentally validated through measurements. Measurements show continuous frequency tuning from 2.38 GHz to 2.67 GHz with an average 10-dB return loss bandwidth of about 170 MHz. Moreover, the antenna maintains good front-to-back ratio in the entire operating band.

INDEX TERMS 3-D printing, composite, conformal, folded dipole, polymer, pure water, tunable.

I. INTRODUCTION

Wireless technology is evolving towards multi-functional, faster, secure and reliable communication systems occupying compact physical dimensions. With the rapid rising demands of compact intelligent systems, antennas having tunable properties are becoming popular. In modern communication systems, reconfigurable antennas have attracted significant interests because of their adaptability of operating frequency, radiation pattern, beam pointing direction, polarization, gain and bandwidth. Reconfigurable antennas can be switched to desired functionalities with the fast-changing operating environments, thus, enhances the reliability of the systems. A single reconfigurable antenna alone can do the jobs of multiple non-tunable antennas. Thus, utilization of reconfigurable antenna in an electronic system reduces hardware size, installation cost and design complexity. Moreover, electromagnetic interference (EMI) among adjacent antennas can be mitigated through replacing multiple antennas of a system by single reconfigurable antenna. Reconfigurable antennas have potential applications in civilian and military communication networks, including cellular networks, satellite and radar communications, aerospace technologies, unmanned airborne vehicle (UAV) radars, smart weapon management and wearable technologies [1].

In literature, extensive research explorations have been conducted on the design and realization of reconfigurable

This article has been accepted for publication in a future issue of this journal, but has not been fully edited. Content may change prior to final publication. Citation information: DOI 10.1109/ACCESS.2021.3114004, IEEE Access

antennas, which primarily focussed on the tunability of resonance frequency [2], radiation pattern [3], [4], polarization [5] and combinations of two or more of these properties [6]. Reconfigurability in antennas' operations are primarily achieved by mechanically tuning antennas' geometries [2], [5], [7] or integrating electronic components, such as varactor diodes [8], PIN diodes [4], [9], photoconducting switches [6] or RF micro-electromechanical (RF-MEM) switches [10] within the antenna structures. These reconfigurable techniques are associated with their own pros and cons [1]. For instance, mechanically reconfigurable antennas do not require bias networks and free from power losses within switching components. However, these antennas are slow response antennas and antenna geometry needs to be altered in reconfigurable operations. On the other hand, electronic reconfigurable antennas are fast response antennas and antenna geometry do not need to be altered for reconfigurable operations, but these antennas suffer from power loss and nonlinearity of the integrated lumped electronic components. In spite of having some limitations, the use of electronic reconfigurable antennas is increasing. Electronic reconfigurable antennas can have continuous or discrete tuning characteristics. Among electronic reconfigurable antenna technologies, RF MEM switches and PIN diodes have discrete tuning capabilities and varactor diodes have continues tuning properties. In this demonstrated research effort, varactor diode is used to design a frequency reconfigurable antenna having continuous frequency tuning from 2.38 to 2.67 GHz.

In various applications of modern wireless communications, antennas are required to be conformal in structures, especially in wearable technologies where antennas are mounted on different parts on human body and exposed to frequent physical deformations [11], [12]. In addition to flexible geometry, unobtrusiveness is also a desirable property of body-worn devices to conceal their appearance. Unobtrusiveness enhances the reliability and aesthetics [13], [14] of wearable devices. It is demonstrated that conformal and transparent wearable devices can be integrated on patients' body with nearly unnoticeable appearance. Unnoticeable sensing technology is an effective method of seamless remote surveillance of patients' health conditions incorporating minimum interruption with their regular activities. It is explicit that sight insensitive wearable devices are becoming influential components in tele-healthcare and mobile healthcare systems. However, significant challenges are associated with the production of robust, flexible and transparent antennas. The significant challenges that should be mentioned are that most of the existing transparent conductive and dielectric materials are not flexible and there is unavoidable trade-off between their light transparency and electrical characteristics, and their fabrication can be complex and expensive [15]. So, effective alternative technologies need to be unveiled to cope up with these challenges. Moreover, for wearable applications, it should be considered that human-body is a frequently variable operating environments for antennas. In many wearable applications, antennas need to be reconfigurable to get best performance in frequently variable on-body platforms. In addition to wearable technologies, reconfigurable flexible transparent antennas have also potential applications in satellite communications, vehicular networks and concealed cellular networks. However, when it is intended to realize reconfigurable antennas that are concurrently flexible and transparent then the challenge is certain degree higher. Maintaining robust integration of the lumped electronic components within antenna geometry in flexible operations is the major realization challenge of active flexible antennas [8]. For these shortcomings, the progress of the development of reconfigurable flexible antennas is quite slow.

In recent years, water is becoming a popular material in antenna fabrication because of its excellent physical, electrical and optical characteristics and easy availability. In the literature, good amount of research studies are visible on water-based antennas, which used either sea water [16]–[19], pure water [20]–[22] or combination of both [23]. So, water is considered as a potential component for the realization of transparent-flexible-robust antennas. In this paper, we have utilized pure water and our recently explored polymer-conductive-mesh composite technology [12], [15] to develop a robust, transparent, flexible, unidirectional and frequency reconfigurable antenna in simple and cost-effective method. To the best of our knowledge, this is the first time such an antenna with all of these features combined together is presented. The radiator of the antenna is a folded dipole made with transparent fabric, which is backed by a water reflector enclosed inside flexible polydimethylsiloxane (PDMS) cavity that alters the omnidirectional radiation of the folded-dipole to directional pattern. Varactor diode is implemented in the radiator to facilitate continuous frequency tunability, which is activated by reverse biased DC voltage, supplied through a bias tee. Due to the tiny size of the varactor diode, its inclusion has insignificant effect on the transparency and flexibility of the antenna. The proposed water-based reconfigurable antenna is fabricated by using 3-D printed molds and the fabricated prototype is experimentally tested in different bias states to evaluate its feasibility in frequency reconfigurable operations.

II. CHARACTERISTICS OF THE MATERIALS

For the demonstrated antenna prototyping, highly flexible and transparent materials are selected. The radiator of the antenna is made with Less EMF Inc's transparent, flexible and stretchable mesh-structured unique conductive fabric VeilShield. VeilShield is structurally uniform e-textile, which is much easier to process than photolithography or inkjet printing technologies. VeilShield comprises woven 132/inch gridded mono-filament polyester yarns electroplated with Zinc-blackened Nickel over Copper. This conductive textile sheet is 57 μm thin, comprises 40 g/m^2 weight and has 0.1 Ω/sq sheet resistance. For accurate modelling of this mesh sheet in simulation analysis, its equivalent sheet resistance after PDMS percolation was estimated through transmission line and T-resonator analysis [15]. From this analysis, the

This article has been accepted for publication in a future issue of this journal, but has not been fully edited. Content may change prior to final publication. Citation information: DOI 10.1109/ACCESS.2021.3114004, IEEE Access

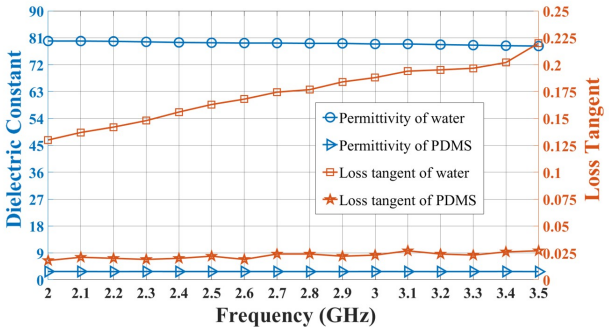

FIGURE 1. Dielectric properties of water and PDMS.

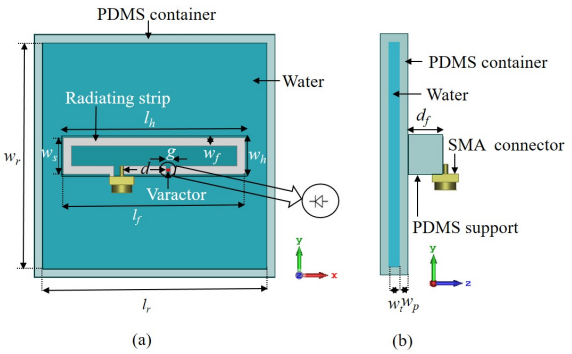

FIGURE 2. Antenna configuration: (a) Top view, (b) Side view.

estimated equivalent sheet resistance of the PDMS penetrated VeilShield sheet was about 0.7 Ω/sq [15], this value was used in the simulation modelling in CST Microwave Studio.

In the proposed design, pure water is used as the planar reflector. Pure water is nearly 100% transparent, high permittivity and bio-friendly liquid. In antenna prototyping, water is contained inside a rectangular container made with PDMS, which has been emerging for the development of flexible electronics for its unique characteristics including biocompatibility, water resistances, excellent flexibility and transparency (i.e., more than 94% [24]). Uncured PDMS is a glutinous dense liquid, which turns into flexible substrate after curing. In our antenna fabrication, PDMS solution was made with Dow Corning Sylgard 184 silicone elastomer kit which comes with base and curing agent, commonly to be mixed at 10:1 ratio. The measured dielectric constant of the PDMS solution is 2.75, which remains almost invariable from 2 to 3.5 GHz frequency band, whereas the measured loss tangent changes from 0.018 to 0.024 in this band of frequency. On the other hand, at room temperature, pure water exhibits much higher dielectric constant and loss tangent. The dielectric constant and loss tangent of the PDMS along with water are depicted in Fig.1, obtained by measuring with Agilent 85070E Dielectric Kit. It can be seen that water has very high dielectric constant, the contrast in dielectric constant between pure water and PDMS leads to the reflection of waves radiated by the folded dipole.

III. ANTENNA TOPOLOGY AND OPERATING MECHANISM

A. ANTENNA TOPOLOGY

Fig. 2 illustrates the configuration of the proposed antenna. The radiating component of the proposed design is a planar off-center-fed folded electric dipole which is positioned on top of the PDMS supporting block and the water reflector layer contained inside the PDMS container. Folded dipole antenna occupies small size, which makes it suitable in compact circuit applications. However, this type of antenna has omnidirectional radiation pattern which is incompatible in many applications where unidirectional patterns are desired, e.g., body-worn applications. Microstrip patch antennas, on the other hand, have the capability of providing unidirectional radiation because of the existence of ground plane. However, if it is intended to design transparent patch antennas then it is hard to achieve high transparency because no transparent metal can achieve very high optical transparency without compromising conductivity. Moreover, the overlapping layer of patch and ground further reduces the overall transparency of the antenna.

Water has almost 100% optical transparency [25], and PDMS, on top of being highly flexible and durable [15], [26], [27], also has high optical transparency of approximately 94% [24]. On the other hand, VeilShield has lower transparency (≈72%) [15] than water and PDMS. In the demonstrated antenna, only the dipole is realized with transparent metal and its dimension occupies a very small portion of the antenna. Moreover, there is no metalized ground plane but water. Such configuration then allows for a realization of flexible antenna with high optical transparency.

The varactor diode is integrated in the radiator as shown in Fig. 2 to tune the resonance frequency. The anode and cathode of the varactor are connected in the radiator as such a direction so that it can be reversed biased by a single DC voltage applied together with the RF input through a bias tee. Thanks to the closed loop structure of the folded dipole, there is no need for an extra connection for DC current flow to the ground as well as the RF choke to isolate the RF and the ground, which is generally required in varactor tuned patch antennas [8]. The simulated surface current distribution of the radiator at 2.38 GHz for the junction capacitance of 1.1pF (the resonance frequency of the antenna is 2.38 GHz for the junction capacitance of 1.1pF, which will be shown later) is illustrated in Fig. 3. The diode is placed at the location of high current density to get good frequency tuning. Upon placement, the varactor is further covered by PDMS to enhance the attachment for robust integration with the antenna.

B. OPERATING MECHANISM

The main radiator of the antenna is an off-center-fed folded dipole which has omnidirectional radiation pattern. The water reflector is located at one side of the folded dipole to

This article has been accepted for publication in a future issue of this journal, but has not been fully edited. Content may change prior to final publication. Citation information: DOI 10.1109/ACCESS.2021.3114004, IEEE Access

TABLE 1. Dimensions of the water-based frequency reconfigurable antenna.

Parameter	Definition	Value (mm)
l_r	Water reflector's length	56
w_r	Water reflector's width	56
w_t	Water reflector's thickness	2.5
w_p	PDMS container's thickness	2
l_h	Length of the PDMS support	46
w_h	Width of the PDMS support	10
d_f	Height of the PDMS support	8
l_f	Length of the folded dipole	45
w_s	Width of the folded dipole	9
w_f	Width of the radiating strip	2
d	Distance from SMA pin to varactor	11
g	Width of the slot containing varactor	1

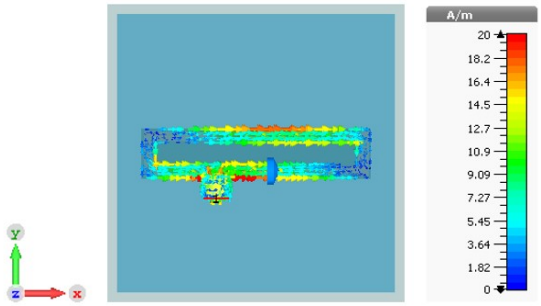

FIGURE 3. Surface current distribution at 2.38 GHz.

transform its omnidirectional radiation pattern to directional broadside pattern. The large difference in the relative permittivity of water and its surrounding media (i.e., air and PDMS) creates an approximate boundary criterion exactly like an electric wall [28]. Hence, the enclosed water acts like a ground plane, reflecting most of radiation coming from the dipole towards +z-axis (broadside), thus, emulating the broadside pattern of microstrip patch antennas.

The width of the dipole strip and position of the feed are optimized to get good impedance matching at the feeding port for the entire operating band of interest. Optimization was accomplished with CST Microwave Studio 2017. The water reflector's dimensions play a significant role in achieving unidirectional pattern. The impacts of the water layer's length, width and thickness on the radiation properties have been investigated and the results are presented in the next section. The optimum dimensions of the antenna are selected based on this parametric investigation; while selecting the parameters, small size of the antenna and satisfactory radiation performance are considered. The optimized dimensions of the antenna configuration selected in our design are shown in Table 1.

To achieve frequency tuning, a GaAs hyperabrupt varactor diode (MGV 125-20-0805-2) from Aeroflex Metelics is used in this design. This diode has good tuning range and low internal resistance [29]. The DC bias supply limit of this varactor diode is 0-20 V. For simulation analysis, the diode is modelled in CST with its equivalent electrical

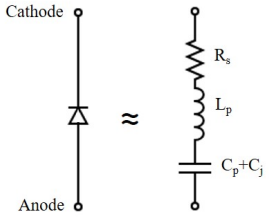

FIGURE 4. Equivalent circuit of the varactor diode.

TABLE 2. Applied reverse bias voltage and the corresponding junction capacitance of the varactor diode. [8].

Bias voltage (V)	0	2	4	6	20
Junction capacitance (pF)	1.1	0.72	0.46	0.34	0.097

circuit as illustrated in Fig. 4 [29]. The equivalent circuit of the varactor diode is comprised of a parasitic inductance (L_p = 0.4 nH), parasitic resistance (R_s = 1.6 Ω), parasitic capacitance (C_p = 0.06 pF) and junction capacitance (C_j). The junction capacitance varies with the variation of supply DC bias voltage. The junction capacitance of the diode for the corresponding DC bias voltage is shown in Table 2. Variation of the supplied reverse bias voltage alters the junction capacitance of the diode, thus, varies the resonance frequency of the antenna. So, continuous frequency tuning is achieved by simply changing the supply DC bias voltage.

IV. PARAMETRIC STUDY

The electromagnetic characteristics of the proposed antenna largely depends on water reflector's length, width, thickness and the gap between dipole radiator and water reflector. The potential impacts of these parameters on antenna behaviour have been computed in CST Microwave Studio and the computed results are exhibited in this paper. The influence of the parameters are investigated for the junction capacitance of 0.46 pF (the resonance frequency of the antenna for 0.46 pF junction capacitance is 2.44 GHz for the dimensions shown in Table 1). It should be noted that for evaluating the influence of one parameter, the remaining parameter values are kept constant at the values given in Table 1.

A. EFFECTS OF WATER REFLECTOR'S LENGTH

The radiation characteristics of the antenna is highly sensitive to the water reflector's length. Fig. 5 demonstrates how the radiation pattern of the antenna changes with the variation of water reflector's length. It can be noticed that larger length of the reflector increases the front radiation (+z- axis) and subsequently decreases the back radiation (-z- axis).

The computed front-to-back (F/B) ratio of the radiation patterns at two principle planes for different water reflector's length are shown in Table 3 which clearly demonstrates the change of F/B ratio with the change of the water reflector's length. The change in F/B ratio is mostly significant at

This article has been accepted for publication in a future issue of this journal, but has not been fully edited. Content may change prior to final publication. Citation information: DOI 10.1109/ACCESS.2021.3114004, IEEE Access

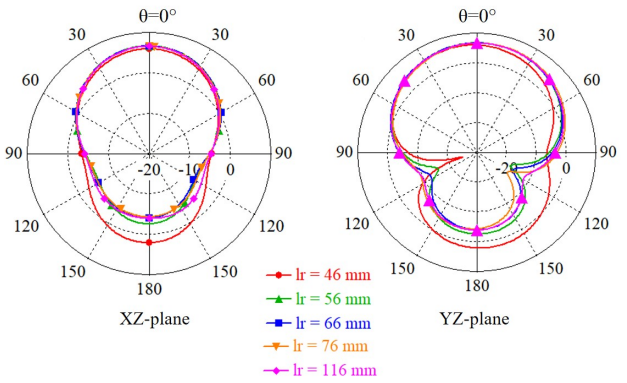

FIGURE 5. The radiation patterns of the antenna at 2.44 GHz for various length of the water reflector.

TABLE 3. Front-to-Back (F/B) ratio for different water reflector's length.

l_r (mm)	46	56	66	76	116
F/B (dB) : XZ-plane	4	9.3	10.7	11	10.4
F/B (dB) : YZ-plane	4	9.3	10.7	10.9	10.6

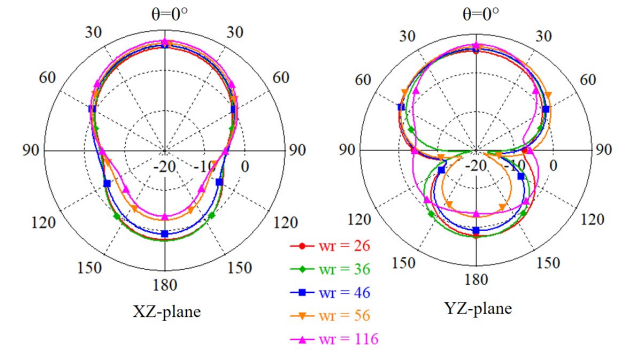

FIGURE 6. The radiation patterns of the antenna at 2.44 GHz for various width of the water reflector.

smaller lengths of the reflector. Targeting for an optimal F/B ratio and less overall size, we have selected 56 mm as the length of the reflector.

B. EFFECTS OF WATER REFLECTOR'S WIDTH

The width of the water reflector has significant effects on the radiation patterns but has insignificant effects on the resonance frequency. Fig. 6 shows the radiation patterns of the antenna at 2.44 GHz for varying the width from 26 mm to 116 mm.

The computed front-to-back (F/B) ratio of the radiation patterns at two principle planes for different water reflector's width are shown in Table 4 which explicitly shows the change of F/B ratio with the change of the water reflector's width, however, for very wide reflector (116 mm), the variation is not very significant. The selected width for the optimum design is 56 mm, which gives good F/B ratio with small antenna size.

TABLE 4. Front-to-Back (F/B) ratio for different water reflector's width.

w_r (mm)	26	36	46	56	116
F/B (dB) : XZ-plane	3.4	3.7	5.4	9.3	11
F/B (dB) : YZ-plane	3.3	3.7	5.4	9.3	8.9

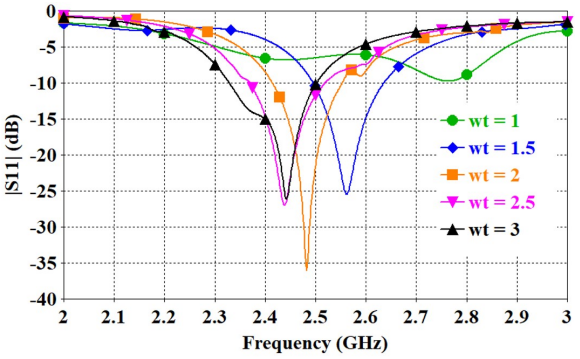

FIGURE 7. The resonance frequency of the antenna for different thickness of the water reflector.

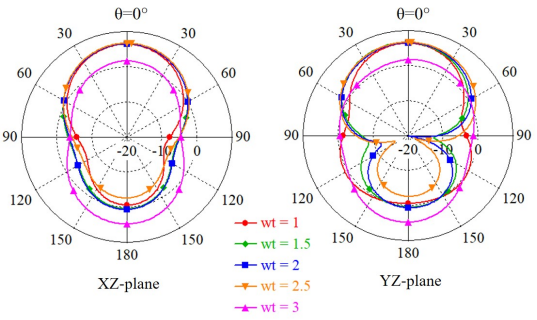

FIGURE 8. The radiation patterns of the antenna for different thickness of the water reflector.

C. EFFECTS OF WATER REFLECTOR'S THICKNESS

Water Reflector's thickness significantly impacts the resonance frequency and radiation patterns. Fig. 7 illustrates that the resonance frequency changes with the change of water-layer thickness. Water has dielectric loading effects on the antenna, with the variation of water reflector's thickness, the loading effect also alters and the resonance frequency shifts accordingly.

The thickness of the water layer has effect on its reflection characteristics, which impacts the radiation pattern of the antenna. The radiation patterns at the corresponding resonance frequencies for various water reflector's thickness values are plotted in Fig. 8 and the corresponding F/B ratio for these thickness values are shown in Table 5. It can be seen that for 2.5 mm thick water layer, good F/B ratio is achieved, this thickness value is selected in our design, it can also be noticed that for 3 mm thickness, the F/B ratio is negative which indicates that main radiation goes towards -z-axis. So, water layer thickness should be selected properly to get the radiation in the desired direction with satisfactory F/B ratio.

This article has been accepted for publication in a future issue of this journal, but has not been fully edited. Content may change prior to final publication. Citation information: DOI 10.1109/ACCESS.2021.3114004, IEEE Access

TABLE 5. Front-to-Back (F/B) ratio for different water reflector's thickness.

w_t (mm)	1	1.5	2	2.5	3
F/B (dB) : XZ-plane	5.6	6.2	5.9	9.3	-2.9
F/B (dB) : YZ-plane	7.1	6.2	5.9	9.3	-3

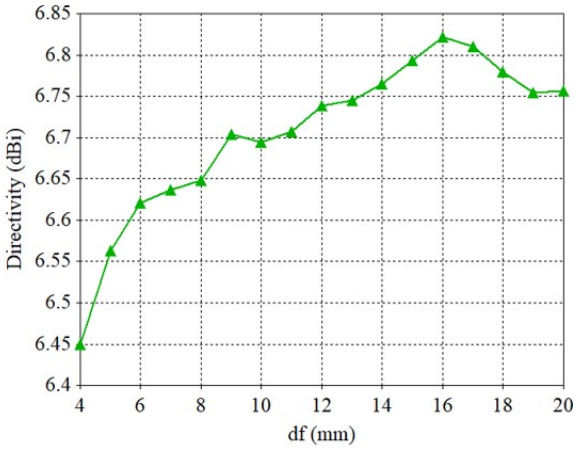

FIGURE 9. The directivity vs frequency of the antenna for different gap between the dipole and reflector surface.

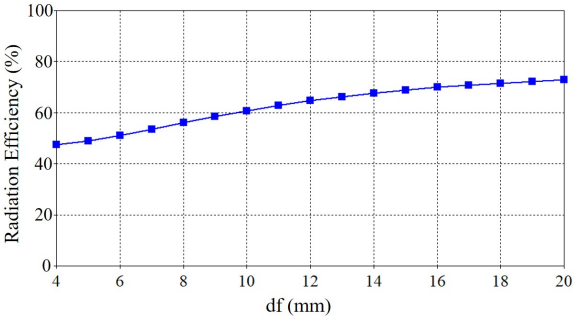

FIGURE 10. Radiation efficiency vs frequency of the antenna for different gap between the dipole and reflector surface.

D. EFFECTS OF THE GAP BETWEEN THE DIPOLE RADIATOR AND REFLECTOR SURFACE

The gap between the dipole radiator and reflector surface (d_f) significantly affects the radiation behaviour of the antenna. The directivity of the antenna at 2.44 GHz for varying the gap between the dipole radiator and reflector surface is shown in Fig. 9. It is demonstrated that maximum directivity is achieved at 16 mm ($\sim \lambda_0/8$) distance, but in our design, 8 mm distance is selected to keep the antenna size compact while maintaining good directivity. The radiation efficiency of the antenna with the increase of the distance from the dipole radiator to reflector surface is illustrated in Fig. 10, which demonstrates the gradual improvement of the efficiency with the increase of the distance, at 8 mm distance, the efficiency is about 56%.

E. PROTOTYPE FABRICATION

The design was prototyped by using three custom designed 3-D printed molds. The molds were fabricated with photo-polymer resin in a Stereolithography (SLA) based 3-D printer (Form 2 from Formlabs). After fabricating the molds in the 3-D printer, antenna prototyping was started. At the initial stage of the fabrication procedure, PDMS solution was made with commercially available Dow Corning's Sylgard 184 silicone elastomer kit by thoroughly mixing base and curing agent at the ratio of 10:1. Then, the uncured PDMS solution was one-by-one poured into the three 3-D printed molds. PDMS solutions in three molds were then simultaneously degassed in a vacuum desiccator to dispel the air bubbles which appeared while mixing the base and curing agent. Next, the PDMS solutions in the three molds were simultaneously cured in an oven by keeping about 3 hours at 60°C. The cured PDMS blocks were then carefully taken out from the molds. Three PDMS blocks were made from these three molds as illustrated in Fig. 11. PDMS block 1 made from mold 1 was a square containing four side walls (see Fig. 11). On the other hand, PDMS block 2 made from mold 2 was a simple plain square (see Fig. 11). When block 2 was attached on top of block 1, a hollow PDMS cavity was formed. Water was injected inside the cavity through the PDMS wall by using a syringe. PDMS block 3 made from mold 3 was a rectangle (see Fig. 11), which was attached on top of the PDMS cavity to support the radiator.

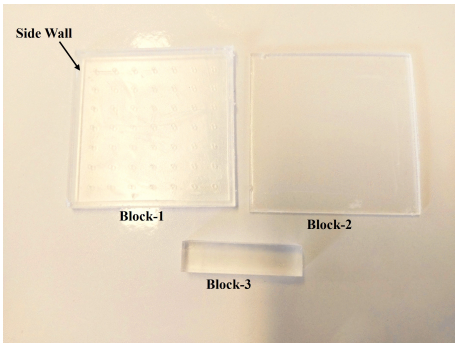

FIGURE 11. Photo of the PDMS blocks made from the 3-D printed molds.

The radiator of the antenna is a folded dipole made from transparent conductive fabric VeilShield. The radiator was made by cutting the VeilShield fabric with a very sharp blade. Then, the varactor diode was connected to the radiator by using MG Chemicals's silver conductive epoxy adhesive (having the resistivity of 0.0007 Ω.cm). To feed the antenna, an SMA connector was connected to it by using silver conductive epoxy adhesive. The fabricated prototype of the antenna is shown in Fig. 12 where the left photo illustrates the high transparency of the prototype by clear readability of the texts and the right photo reveals its high flexibility through bending to a low radius curvature.

V. NUMERICAL AND EXPERIMENTAL PERFORMANCE INVESTIGATION

The proposed antenna was numerically analysed and experimentally tested for evaluating the validation of the design.

This article has been accepted for publication in a future issue of this journal, but has not been fully edited. Content may change prior to final publication. Citation information: DOI 10.1109/ACCESS.2021.3114004, IEEE Access

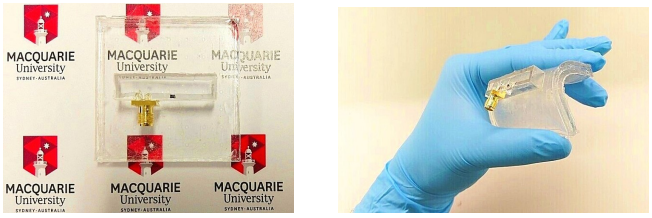

FIGURE 12. Photos of the antenna prototype: (a) flat state, (b) bent state.

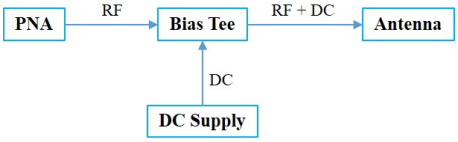

FIGURE 13. Schematic diagram of the measurement procedure of the antenna by simultaneously coupling the applied RF and DC supply through the bias tee.

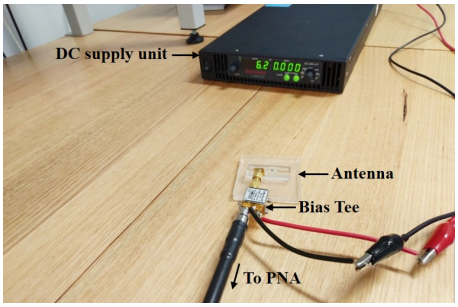

FIGURE 14. The input reflection coefficient measurement set-up for the antenna.

The simulation investigation was conducted for the junction capacitance 1.1pF, 0.72pF, 0.46pF, 0.34pF and 0.097pF for the corresponding DC bias voltage of 0V, 2V, 4V, 6V and 20V, respectively.

To validate the design, measurements were also conducted at five bias voltage stages. The input reflection coefficient ($|S_{11}|$) was measured in Agilent PNA-X N5242A network analyzer, calibrated by an electronic calibration module N4691B from Keysight. The reverse bias voltage was supplied by a DC power source (XG 300-2.8 from Sorensen). The DC supply was varied from 0 to 20V. The RF and DC supplies were coupled in a bias tee and fed the antenna. The use of bias tee avoids the need of complex biasing circuit that often comes with extra cables. Such additions often not only affect the antenna flexibility, but also its radiation performance. The schematic diagram of the measurement setting of the antenna with the bias tee and DC power supply is illustrated in Fig. 13. Fig. 14 shows the photograph of the $|S_{11}|$ measurement set-up of the antenna. It can be noted that the external bias tee is used here for simplicity in measurement for concept demonstration, in actual application scenarios, integrated bias tee can be used.

The predicted and measured results of $|S_{11}|$ at five bias

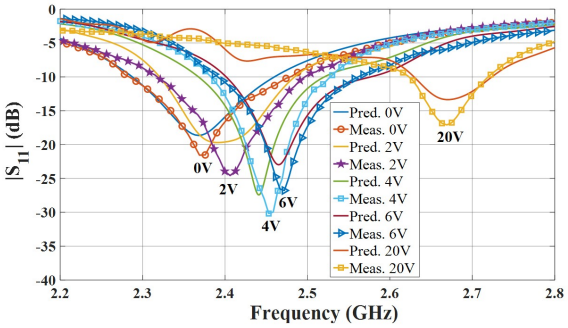

FIGURE 15. Predicted and measured $|S_{11}|$ of the proposed antenna at different bias states.

states are depicted in Fig. 15. The predicted $|S_{11}|$ are shown for the five junction capacitance values and the measured results are the $|S_{11}|$ for the corresponding DC bias voltages. The simulation results depict that the resonance frequency shifts with the change of the junction capacitance, which explicitly confirms the idea of frequency tuning operation. Moreover, promising similarity is visible between the predicted and measured results, confirming the validation of the design. The small variance in results attributes to the fabrication tolerance. The results of Fig. 15 exhibit that with the increase of DC bias voltage (decreasing junction capacitance), resonance frequency shifts to higher band. The observed resonance frequency tuning range of the antenna is from 2.38 to 2.67 GHz with an average 10-dB return loss bandwidth of about 170 MHz. It can be noticed that frequency tuning operation is achieved by the varactor diode with good matching and bandwidth at every bias state.

The far-field radiation patterns of the antenna were measured in NSI700S-50 spherical near-field antenna range. Like $|S_{11}|$ measurements, the reverse bias voltage was supplied by a DC power source (XG 300-2.8 from Sorensen), the RF and DC supplies were coupled through the bias tee. Fig. 16 and Fig. 17 represent the measured normalized radiation patterns at 2.38 GHz and 2.67 GHz for the applied DC bias voltage of 0V and 20V, respectively. The patterns show that the antenna radiates at broadside direction like a microstrip patch antenna, thus, validates the proposed design. Similar broadside patterns are maintained at the intermediate bias states also, which are not shown here for clarity.

The corresponding resonance frequency, peak gain, and efficiency of the antenna at different bias states are exhibited in Table 6. The results explicitly state that the explored technique can be implemented for frequency tuning operations in transparent flexible antennas.

VI. LOSS ANALYSIS OF THE ANTENNA

The above investigation exhibits that the demonstrated frequency reconfigurable antenna achieved an efficiency between 48.3% to 57.7%. It is worthy to investigate the major factors contributing to the losses of the antenna and, thus, identify the possible solution to minimize the losses and in-

This article has been accepted for publication in a future issue of this journal, but has not been fully edited. Content may change prior to final publication. Citation information: DOI 10.1109/ACCESS.2021.3114004, IEEE Access

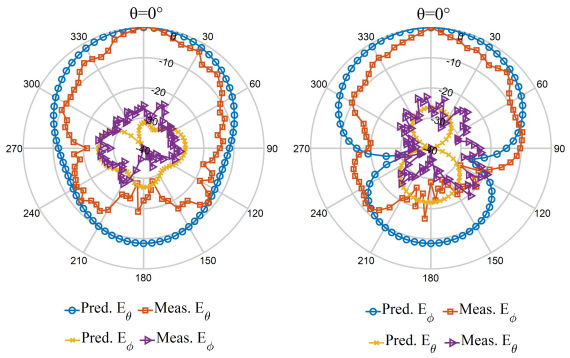

FIGURE 16. Predicted and measured far-field radiation patterns of the proposed antenna at 2.38 GHz for the applied bias voltage of 0V. (a) XZ-plane, (b) YZ-plane.

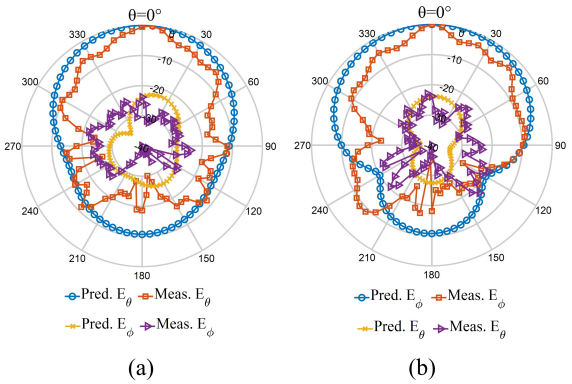

FIGURE 17. Predicted and measured far-field radiation patterns of the proposed antenna at 2.67 GHz for the applied bias voltage of 20V. (a) XZ-plane, (b) YZ-plane.

crease the efficiency. A simulation investigation is conducted for each bias state and loss occurs in the individual material at the corresponding resonance frequency is observed, which is depicted in Table 7. From this loss analysis, it is observed that at every bias state, VeilShield contributes major power loss which is more than 30%, on the other hand, nearly 10% power is lost in PDMS at each bias state. Water contributes negligible loss compared to VeilShield and PDMS. It can be noted that the main radiator of the antenna is the folded dipole made with VeilShield which has much higher resistance (0.7 Ω/sq equivalent sheet resistance after PDMS percolation) than the traditional rigid conductors. The high resistance is responsible for most of the power loss of the antenna. However, despite the lossy nature, VeilShield-PDMS composite can be a potential substitute for the development of transparent-conformal antennas because of its remarkable characteristics of high transparency, robustness and easy processing. These characteristics cannot be found simultaneously in other transparent materials. In future, more research explorations can be conducted to increase the efficiency by reducing the losses contributed by the associated materials. One possible approach for reducing the loss of the PDMS can be doping it with low loss micro-particles, e.g., glass microspheres, the similar approach as utilized by [30] in millimeter-wave band. Another possibility is to improve the conductivity of the transparent fabric, for instance through multiple conductive coating of the fabric [31].

TABLE 6. Antenna performance at different bias states.

Bias voltage (V)	0	2	4	6	20
Resonance frequency (GHz)	2.38	2.4	2.44	2.47	2.67
Predicted peak gain (dBi)	3.52	3.68	4.11	4.25	2.45
Measured peak gain (dBi)	3.27	3.5	3.92	4.07	2.28
Predicted efficiency (%)	48.3	48.5	55.6	57.7	53.6
Measured efficiency (%)	44.1	47.7	53.8	56.5	50.4

VII. COMPARISON AND DISCUSSION

The numerical analysis and experimental results certainly reveal that the proposed antenna can be an excellent candidate of frequency reconfigurable flexible and transparent antenna. It is worthy to conduct a performance comparison with other state-of-the-art water-based reconfigurable transparent antennas to demonstrate the advantages of the proposed design. Table 8 exhibits the comparison of the proposed antenna with some recent water-based reconfigurable antennas, this comparison includes tuning parameters, mechanism to achieve parameter tuning, types of water used in antenna designs, transparency and flexibility of the antennas and the materials used in the water holders. It is ascertained that the reported reconfigurable water antennas in literature are not simultaneously transparent and flexible. Moreover, to the best of our knowledge, our proposed antenna is the first reported transparent and flexible water-based antenna integrating active electronic component for frequency tuning operation. In addition, it can also be noted that some transparent water antennas demonstrated in Table 8 (i.e., [32], [33] and [37]) have opaque rigid ground planes, so these antennas are not entirely transparent. In contrast to these designs, our explored design has used water reflector to form unidirectional radiation, in this design, the main radiator is made from transparent fabric which makes the prototype entirely transparent and flexible. In comparison to other water-based reconfigurable antennas, our proposed antenna incorporates some remarkable characteristics (i.e., realized from transparent and flexible conductive and dielectric materials, integration of tiny varactor diode to achieve frequency tuning, unidirectional pattern by using water reflector contained inside transparent-flexible container) which position it as a unique design.

VIII. CONCLUSION

A unique design of active frequency reconfigurable antenna is demonstrated in this paper. The investigated antenna has highly flexible and robust structure, excellent optical transparency and unidirectional radiation pattern. The antenna is manufactured from flexible, robust, easily available and low-cost materials. The main radiator of the antenna is a folded dipole made from flexible transparent fabric and backed by a

TABLE 7. Loss in different materials at different bias states of the varactor diode.

Bias voltage (V)	Resonance frequency (GHz)	Loss in VeilShield (%)	Loss in PDMS (%)	Loss in Water (%)
0	2.38	39	12	7.76e-4
2	2.4	38	12	2.04e-4
4	2.44	34	10	1.3e-4
6	2.47	32	10	1.03e-4
20	2.67	36	10	1.03e-4

TABLE 8. Performance comparison with previous water-based reconfigurable antennas.

Ref.	Tuning Parameter	Tuning Mechanism	Water Type	Transparent	Flexible	Water Holder Material
[32]	Polarization	Mechanical	Pure	Yes	No	Glass
[33]	Frequency	Mechanical	Pure	Yes	No	Acrylic
[34]	Frequency	Mechanical	Pure and Salt	Yes	No	Plexiglass
[35]	Polarization and Frequency	Mechanical	Pure	No	No	PVC
[36]	Pattern	Mechanical	Pure	No	No	Photopolymer resin
[37]	Frequency	Mechanical	Salt	Yes	No	Acrylic
[38]	Pattern	Mechanical	Pure	No	No	Glass
[21]	Frequency	Mechanical	Pure	No	No	Plastic
This Work	Frequency	Electronic	Pure	Yes	Yes	Polymer

water reflector which transforms the omnidirectional pattern of the folded-dipole to unidirectional broadside pattern. Frequency tuning operation is achieved by incorporating a tiny varactor diode in the main body of the radiator. Integration of the varactor diode in the folded dipole avoids the requirement of extra bias circuity, thus, improves design simplicity and radiation purity. The equivalent junction capacitance of the varactor diode varies with the change of supply DC bias voltage, which in turn switches the operating frequency of the antenna. By controlling the supply DC bias voltage, the resonance frequency of the antenna can be adjusted to the desired level. The measured results of the fabricated prototype exhibit promising performance. It is revealed that the explored design can be implemented to develop low-cost, electronically tunable, visually imperceptible, robust, flexible and unidirectional antennas. In future, alternative liquids can be investigated which have a comparable electrical and physical properties with water and are not reactive to PDMS, and to compare the antenna performance with those liquids.

ACKNOWLEDGEMENT

The authors would like to thank Hangrui Liu, Department of Physics and Astronomy, Macquarie University, Sydney, Australia for fabricating the molds. The authors acknowledge financial support from Australian Research council Discovery grant scheme and University of Technology Sydney Faculty of Engineering and IT Seed Grant.

REFERENCES

[1] N. Haider, D. Caratelli, and A. G. Yarovoy, "Recent Developments in Reconfigurable and Multiband Antenna Technology," *International Journal of Antennas and Propagation*, vol. 2013, p. 869170, Mar 2013.

[2] S. J. Chen, D. C. Ranasinghe, and C. Fumeaux, "A Robust Snap-On Button Solution for Reconfigurable Wearable Textile Antennas," *IEEE Transactions on Antennas and Propagation*, vol. 66, no. 9, pp. 4541–4551, 2018.

[3] P. Qin, Y. J. Guo, A. R. Weily, and C. Liang, "A Pattern Reconfigurable U-Slot Antenna and Its Applications in MIMO Systems," *IEEE Transactions on Antennas and Propagation*, vol. 60, no. 2, pp. 516–528, 2012.

[4] G. Yang, J. Li, D. Wei, S. Zhou, and R. Xu, "Pattern Reconfigurable Microstrip Antenna With Multidirectional Beam for Wireless Communication," *IEEE Transactions on Antennas and Propagation*, vol. 67, no. 3, pp. 1910–1915, 2019.

[5] C. Wang, J. C. Yeo, H. Chu, C. T. Lim, and Y. Guo, "Design of a Reconfigurable Patch Antenna Using the Movement of Liquid Metal," *IEEE Antennas and Wireless Propagation Letters*, vol. 17, no. 6, pp. 974–977, 2018.

[6] C. J. Panagamuwa, A. Chauraya, and J. C. Vardaxoglou, "Frequency and beam reconfigurable antenna using photoconducting switches," *IEEE Transactions on Antennas and Propagation*, vol. 54, no. 2, pp. 449–454, 2006.

[7] T. Jang, C. Zhang, H. Youn, J. Zhou, and L. J. Guo, "Semitransparent and flexible mechanically reconfigurable electrically small antennas based on tortuous metallic micromesh," *IEEE Transactions on Antennas and Propagation*, vol. 65, no. 1, pp. 150–158, Jan 2017.

[8] R. B. V. B. Simorangkir, Y. Yang, K. P. Esselle, and B. A. Zeb, "A method to realize robust flexible electronically tunable antennas using polymer-embedded conductive fabric," *IEEE Transactions on Antennas and Propagation*, vol. 66, no. 1, pp. 50–58, Jan 2018.

[9] Y. Yang, R. B. V. B. Simorangkir, X. Zhu, K. Esselle, and Q. Xue, "A Novel Boresight and Conical Pattern Reconfigurable Antenna With the Diversity of 360° Polarization Scanning," *IEEE Transactions on Antennas and Propagation*, vol. 65, no. 11, pp. 5747–5756, 2017.

[10] G. Wang, R. Bairavasubramanian, B. Pan, and J. Papapolymerou, "Radiofrequency MEMS-enabled polarisation reconfigurable antenna arrays on multilayer liquid crystal polymer," *IET Microwaves, Antennas Propagation*, vol. 5, no. 13, pp. 1594–1599, 2011.

[11] P. S. Hall, Y. Hao, Y. I. Nechayev, A. Alomainy, C. C. Constantinou, C. Parini, M. R. Kamarudin, T. Z. Salim, D. T. M. Hee, R. Dubrovka, A. S. Owadally, W. Song, A. Serra, P. Nepa, M. Gallo, and M. Bozzetti, "Antennas and propagation for on-body communication systems," *IEEE Antennas Propag. Mag.*, vol. 49, no. 3, pp. 41–58, June 2007.

[12] A. S. M. Sayem, K. P. Esselle, and R. M. Hashmi, "Increasing the transparency of compact flexible antennas using defected ground structure for unobtrusive wearable technologies," *IET Microwaves, Antennas & Propagation*, vol. 14, pp. 1869–1877(8), November 2020.

[13] Y. Zheng, X. Ding, C. C. Y. Poon, B. P. L. Lo, H. Zhang, X. Zhou, G. Yang, N. Zhao, and Y. Zhang, "Unobtrusive Sensing and Wearable Devices for Health Informatics," *IEEE Transactions on Biomedical Engineering*, vol. 61, no. 5, pp. 1538–1554, May 2014.

[14] R. Paradiso, G. Loriga, and N. Taccini, "A wearable health care system based on knitted integrated sensors," *IEEE Transactions on Information Technology in Biomedicine*, vol. 9, no. 3, pp. 337–344, Sep. 2005.

[15] A. S. M. Sayem, R. B. V. B. Simorangkir, K. P. Esselle, and R. M. Hashmi, "Development of Robust Transparent Conformal Antennas Based on Conductive Mesh-Polymer Composite for Unobtrusive Wearable Applications," *IEEE Transactions on Antennas and Propagation*, vol. 67, no. 12, pp. 7216–7224, Dec 2019.

[16] C. Hua and Z. Shen, "Shunt-excited sea-water monopole antenna of high efficiency," *IEEE Transactions on Antennas and Propagation*, vol. 63, no. 11, pp. 5185–5190, Nov 2015.

[17] C. Hua, Z. Shen, and J. Lu, "High-efficiency sea-water monopole antenna for maritime wireless communications," *IEEE Transactions on Antennas and Propagation*, vol. 62, no. 12, pp. 5968–5973, Dec 2014.

[18] L. Xing, Y. Huang, S. S. Alja'afreh, and S. J. Boyes, "A monopole water antenna," in *2012 Loughborough Antennas Propagation Conference (LAPC)*, Nov 2012, pp. 1–4.

[19] H. Fayad and P. Record, "Broadband liquid antenna," *Electronics Letters*, vol. 42, no. 3, pp. 133–134, Feb 2006.

[20] A. S. M. Sayem, R. B. V. B. Simorangkir, K. P. Esselle, R. M. Hashmi, and H. Liu, "A Method to Develop Flexible Robust Optically Transparent Unidirectional Antennas Utilizing Pure Water, PDMS, and Transparent Conductive Mesh," *IEEE Transactions on Antennas and Propagation*, vol. 68, no. 10, pp. 6943–6952, 2020.

[21] S. G. O'Keefe and S. P. Kingsley, "Tunability of liquid dielectric resonator antennas," *IEEE Antennas and Wireless Propagation Letters*, vol. 6, pp. 533–536, 2007.

[22] R. Zhou and H. Zhang and H. Xin, "Liquid-based dielectric resonator antenna and its application for measuring liquid real permittivities," *IET Microwaves, Antennas Propagation*, vol. 8, no. 4, pp. 255–262, March 2014.

[23] M. Wang and Q. Chu, "High-efficiency and wideband coaxial dual-tube hybrid monopole water antenna," *IEEE Antennas and Wireless Propagation Letters*, vol. 17, no. 5, pp. 799–802, May 2018.

[24] S. Sun, Z. Pan, F. K. Yang, Y. Huang, and B. Zhao, "A transparent silica colloidal crystal/PDMS composite and its application for crack suppression of metallic coatings," *Journal of Colloid and Interface Science*, vol. 461, pp. 136 – 143, 2016. [Online]. Available: http://www.sciencedirect.com/science/article/pii/S0021979715301855

[25] R. Saidur, T. Meng, Z. Said, M. Hasanuzzaman, and A. Kamyar, "Evaluation of the effect of nanofluid-based absorbers on direct solar collector," *International Journal of Heat and Mass Transfer*, vol. 55, no. 21, pp. 5899 – 5907, 2012. [Online]. Available: http://www.sciencedirect.com/science/article/pii/S0017931012004188

[26] A. S. M. Sayem, K. P. Esselle, R. M. Hashmi, and H. Liu, "Experimental studies of the robustness of the conductive-mesh-polymer composite towards the development of conformal and transparent antennas," *Smart Materials and Structures*, vol. 29, no. 8, p. 085015, July 2020.

[27] A. S. M. Sayem, D. Le, R. B. V. B. Simorangkir, T. Björninen, K. P. Esselle, R. M. Hashmi, and M. Zhadobov, "Optically Transparent Flexible Robust Circularly Polarized Antenna for UHF RFID Tags," *IEEE Antennas and Wireless Propagation Letters*, vol. 19, no. 12, pp. 2334–2338, 2020.

[28] H. W. Lai, K. Luk, and K. W. Leung, "Dense Dielectric Patch Antenna-A New Kind of Low-Profile Antenna Element for Wireless Communications," *IEEE Transactions on Antennas and Propagation*, vol. 61, no. 8, pp. 4239–4245, Aug 2013.

[29] A. R. Weily, T. S. Bird, and Y. J. Guo, "A Reconfigurable High-Gain Partially Reflecting Surface Antenna," *IEEE Transactions on Antennas and Propagation*, vol. 56, no. 11, pp. 3382–3390, 2008.

[30] W. A. W. Muhamad, R. Ngah, M. F. Jamlos, P. J. Soh, and M. T. Ali, "High-gain dipole antenna using polydimethylsiloxane–glass microsphere (PDMS-GM) substrate for 5G applications," *Appl. Physics A*, vol. 123, no. 1, p. 102, Dec 2016.

[31] Y. Bayram, Y. Zhou, B. S. Shim, S. Xu, J. Zhu, N. A. Kotov, and J. L. Volakis, "E-textile conductors and polymer composites for conformal lightweight antennas," *IEEE Trans. Antennas Propag.*, vol. 58, no. 8, pp. 2732–2736, Aug 2010.

[32] Z. Hu, S. Wang, Z. Shen, and W. Wu, "Broadband Polarization-Reconfigurable Water Spiral Antenna of Low Profile," *IEEE Antennas and Wireless Propagation Letters*, vol. 16, pp. 1377–1380, 2017.

[33] M. Zou, Z. Shen, and J. Pan, "Frequency-reconfigurable water antenna of circular polarization," *Applied Physics Letters*, vol. 108, no. 1, p. 014102, 2016.

[34] J. Li, J. Fang, J. Dong, and S. Du, "A Transparent Frequency-Reconfigurable Monopole Water Antenna based on Dielectric Resonator," in *2020 International Conference on Microwave and Millimeter Wave Technology (ICMMT)*, 2020, pp. 1–3.

[35] Y.-H. Qian and Q.-X. Chu, "A Polarization-Reconfigurable Water-Loaded Microstrip Antenna," *IEEE Antennas and Wireless Propagation Letters*, vol. 16, pp. 2179–2182, 2017.

[36] J.-J. Liang, G.-L. Huang, K.-W. Qian, S.-L. Zhang, and T. Yuan, "An Azimuth-Pattern Reconfigurable Antenna Based on Water Grating Reflector," *IEEE Access*, vol. 6, pp. 34 804–34 811, 2018.

[37] C. Hua, Z. Shen, and J. Lu, "High-Efficiency Sea-Water Monopole Antenna for Maritime Wireless Communications," *IEEE Transactions on Antennas and Propagation*, vol. 62, no. 12, pp. 5968–5973, 2014.

[38] Z. Hu, Z. Shen, and W. Wu, "Reconfigurable Leaky-Wave Antenna Based on Periodic Water Grating," *IEEE Antennas and Wireless Propagation Letters*, vol. 13, pp. 134–137, 2014.